Physica D 398 (2019) 1–12

Contents lists available at ScienceDirect

Physica D

journal homepage: www.elsevier.com/locate/physd

Dynamics of coupled generators of quasiperiodic oscillations: Different types of synchronization and other phenomena

A.P. Kuznetsov [a], S.P. Kuznetsov [a], N.A. Shchegoleva [b], N.V. Stankevich [a,c,d,*]

[a] Kotel'nikov's Institute of Radio-Engineering and Electronics of RAS, Saratov Branch, Zelenaya 38, Saratov, 410019, Russian Federation
[b] Chernyshevsky Saratov State University, Astrakhanskaya, 83, Saratov, 410012, Russian Federation
[c] Yuri Gagarin State Technical University of Saratov, Politehnicheskaya 77, Saratov, 410054, Russian Federation
[d] St. Petersburg State University, Universitetskiy proezd, 28, Peterhof, Saint-Petersburg, 198504, Russian Federation

HIGHLIGHTS

- Dynamics of coupled generators of quasiperiodic oscillations is investigated.
- Different types of synchronization are observed: complete, phase and broadband synchronization.
- The complex picture of the multi-frequency quasiperiodic oscillations including the Arnold resonance web is revealed.

ARTICLE INFO

Article history:
Received 18 January 2019
Received in revised form 29 May 2019
Accepted 31 May 2019
Available online 6 June 2019
Communicated by H. Nakao

Keywords:
Quasiperiodic oscillations
Coupled generators
Synchronization

ABSTRACT

A problem of synchronization of quasiperiodic oscillations is discussed in application to an example of coupled systems with autonomous quasiperiodic dynamics. Charts of Lyapunov exponents are presented that reveal characteristic domains on the parameter plane such as oscillator death, complete synchronization, phase synchronization of quasiperiodic oscillations, broadband synchronization, broadband quasiperiodicity. Features of each kind of dynamical behavior are discussed. Analysis of corresponding bifurcations is presented, including quasiperiodic Hopf bifurcations, saddle–node bifurcations of invariant tori of different dimensions, and bifurcations of torus doublings. Both the case of dominance of quasiperiodic oscillations in one of the generators and the case of pronounced periodic resonances embedded in the region of quasiperiodicity are considered.

1. Introduction

Nowadays, many examples of generators of periodic and chaotic oscillations are known [1–22]. Generators of periodic oscillations have become classic examples in nonlinear science and are widely used in applications. Chaos generators are of interest in such areas as information and communication systems [6,7], electronic countermeasure systems [8] and noise radar [9], generation of random numbers [10,11], cryptographic applications [12]. Despite a large number of known examples, more and more variants of chaos generators are proposed (see, for instance, [20–22]).

At the same time, there are a few examples of low-dimensional autonomous generators demonstrating quasiperiodic oscillations[1] [23–28]. Quasiperiodic oscillations occupy in a sense an intermediate position between periodic and chaotic oscillations. Quasiperiodic oscillations can be characterized by a number of incommensurate basic frequencies, so that one can talk of two-, three-, four-frequency quasiperiodicity etc. In phase space of a dynamical system the multi-frequency quasiperiodicity corresponds to invariant tori of respective dimensions.

Quasiperiodic oscillations attract attention of researchers since they greatly enrich the fundamental concepts concerning dynamics of self-oscillating systems. Such phenomena as forced synchronization of quasiperiodic oscillations [29–32], bifurcations of invariant tori [33–35], Arnold resonance web [34,36], self-organizing quasiperiodicity [37–39], occurrence of the Landau–Hopf scenario [40], quasiperiodicity with different number of incommensurate frequencies for coupled subsystems with chaotic dynamics [41], were revealed and studied. Of particular interest are problems of quasiperiodicity of different dimensions in coupled discrete-time systems (maps) [42–45].

In this context, the problem of interaction of quasiperiodic generators looks as a logical continuation of studies undertaken in Refs. [46,47] devoted to a four-dimensional modified Anishchenko–Astakhov's generator. Some significant results were obtained, although only cases of small frequency detuning and of small

* Corresponding author at: Yuri Gagarin State Technical University of Saratov, Politehnicheskaya 77, Saratov, 410054, Russian Federation.
E-mail address: stankevichnv@mail.ru (N.V. Stankevich).

[1] Here we talk specifically on autonomous systems; the non-autonomous systems and coupled systems form another class and are much more common.

https://doi.org/10.1016/j.physd.2019.05.014
0167-2789/

coupling strength were examined, and a two-parametric analysis was missed. Note that two-parameter analysis for such tasks is important and informative, since it allows visualizing areas of various types of dynamics in the system parameter space, which can be quite diverse and nontrivial.

Besides purely theoretical interest, it is worth noting prevalence of quasiperiodic dynamics and associated phenomena in engineering, for example, in optoelectronics and lasers [24,48,49], magnetic films [50–53], klystron generators [54,55] etc. In a recent paper [56] some features of formation of bursting dynamics in a single neuron model via torus break-down was described. Fundamental aspects of synchronization of quasiperiodic oscillations are important not only for the theory of oscillations, but also for applications, say, for analyzing interaction of optoelectronic systems, laser systems, and so on. In Ref. [57] some particular questions of synchronization of semiconductor lasers were considered although the authors did not touch on all relevant aspects. In the paper [58] considering the problem of synchronization of quasiperiodic oscillations in an experiment with a thermoacoustic system the authors get only a small part of the picture of synchronization of quasiperiodic oscillations, namely, the phase synchronization. Also, in the context of neuron models it is important to take into consideration the quasiperiodic dynamics, and different effects connected with it.

For analysis of general picture of synchronization the most appropriate is using as a base a simple model with minimal dimension of the phase space, which would allow a good physical interpretation, and manifest interesting dynamics, reach and rough enough in respect to variations of parameters.

In [27] a three-dimensional system generating quasiperiodic oscillations was proposed, and occurrence of autonomous quasiperiodic dynamics in wide parameter ranges was demonstrated. A disadvantage of this model is a specific feature — absence of an equilibrium state, which suggests some limitations in its physical applications.

In the present work, investigating the coupled generators of quasiperiodic oscillations, we prefer to turn to another basic element, namely, the modification of the generator proposed in [28], which possesses an equilibrium state. The dynamics of coupled systems of such kind have many aspects that deserve deep and careful consideration. Say, parameters of the first subsystem may be chosen to provide quasiperiodic oscillations, while those of the second subsystem may correspond to a basic limit cycle, or quasiperiodic oscillations occurring on its base, or resonance limit cycles on respective invariant torus. Features of dynamics of coupled oscillators should be considered naturally depending on the coupling strength and detuning of the basic frequencies of the subsystems. These questions are addressed in the present paper.

2. Dynamics of generator of quasiperiodic oscillations with a single equilibrium state

In [28] a generator of autonomous quasiperiodic oscillations was proposed described by the equations

$$\begin{aligned} &\ddot{x} - (\lambda + z + x^2 - \beta x^4)\dot{x} + \omega_0^2 x = 0, \\ &\dot{z} = b(\varepsilon - z) - k\dot{x}^2. \end{aligned} \tag{1}$$

The model (1) in accordance with [59] is a particular example of an oscillator with inertial self-excitation, concretely, a self-oscillator with hard excitation, in which the supply circuit is inertial, with some characteristic time. The model (1) is a three-dimensional dynamical system, where x, $y = \dot{x}$, z are the state variables. The parameter ε characterizes supply of energy from the power source, the parameter b is a characteristic of inertial properties of the supply circuit. A term containing the coefficient k is responsible for determination of energy level in the self-oscillator. The model (1) has one equilibrium state:

$$x_0 = 0, y_0 = 0, z_0 = \varepsilon. \tag{2}$$

Using standard methods, it is not difficult to show that the equilibrium state can undergo the Andronov–Hopf bifurcation of the birth of limit cycle at the condition

$$\lambda = -\varepsilon. \tag{3}$$

Fig. 1 shows charts of Lyapunov exponents of the system (1) on a plane of the basic frequency vs the parameter responsible for the Andronov–Hopf bifurcation (ω_0, λ), with other parameters fixed: $\varepsilon = 4$, $b = 1$, $k = 0.02$. The parameters are chosen in such way that quasiperiodic oscillations can be observed stable to variations of other parameters. Two values $\beta = 1/18$ (a) and $\beta = 1/25$ (b) are considered. The legend is shown as rectangles stained in respective colors. Details of interpretation of dynamical behaviors basing on the computations of Lyapunov exponents see in the Appendix.

On the charts, one can see the Andronov–Hopf bifurcation line (3), which is the boundary between the domains E and P, and which corresponds to the equality $\lambda = -4$ for the chosen parameter values. In the domain of existence of the basic limit cycle P, a sufficiently wide tongue of autonomous quasiperiodic oscillations T is embedded, and tongues of periodic regimes are observed within this domain of quasiperiodicity. At $\beta = 1/18$, these tongues are very narrow, and in the chart of Fig. 1a they are practically indistinguishable. At $\beta = 1/25$ the tongues are much more pronounced. They correspond to resonant cycles of different periods on the invariant torus. The numbers in the diagram Fig. 1b indicate periods of several cycles defined for the corresponding Poincaré map. Fig. 1 also presents phase portraits of the basic limit cycle in the domain P (Fig. 1c), the invariant torus in the domain T (Fig. 1d), and the resonance cycles on the torus with period 7 (Fig. 1e) and 4 (Fig. 1f). Note that for a cycle of period 4, a pair of cycles simultaneously coexist within the tongue, symmetric to each other in the phase space in accordance with the replacement of the variables ($x \to -x, y \to -y, z \to z$), while the cycle of period 7 has inner symmetry. Features of dynamics in a similar generator with such kind of symmetry were described in [60].

3. Dynamics of coupled generators. Different types of synchronization

A classical case of synchronization is the frequency adjustment of interacting self-oscillatory systems [61]. To study synchronization between quasiperiodic oscillators we will consider dynamics of two dissipatively coupled generators (1) governed by equations

$$\begin{aligned} &\ddot{x}_1 - (\lambda_1 + z_1 + x_1^2 - \beta x_1^4)\dot{x}_1 + \omega_0^2 x_1 + M_C(\dot{x}_1 - \dot{x}_2) = 0, \\ &\dot{z}_1 = b(\varepsilon - z_1) - k\dot{x}_1^2, \\ &\ddot{x}_2 - (\lambda_2 + z_2 + x_2^2 - \beta x_2^4)\dot{x}_2 + (\omega_0 + \Delta)^2 x_2 + M_C(\dot{x}_2 - \dot{x}_1) = 0, \\ &\dot{z}_2 = b(\varepsilon - z_2) - k\dot{x}_2^2, \end{aligned} \tag{4}$$

where x_1, z_1 are variables relating to the first subsystem, and x_2, z_2 are variables of the second subsystem, Δ is parameter of the frequency detuning, M_C is a coefficient of dissipative coupling. Also, we will use further the variables $y_1 = \dot{x}_1$, $y_2 = \dot{x}_2$.

First of all, let us discuss a choice of parameters of the individual generators and start with the case $\beta = 1/18$. Fig. 1a allows choosing the regime of the first individual oscillator corresponding to quasiperiodic oscillations T, for example, $\lambda = -1$ and $\omega_0 =$

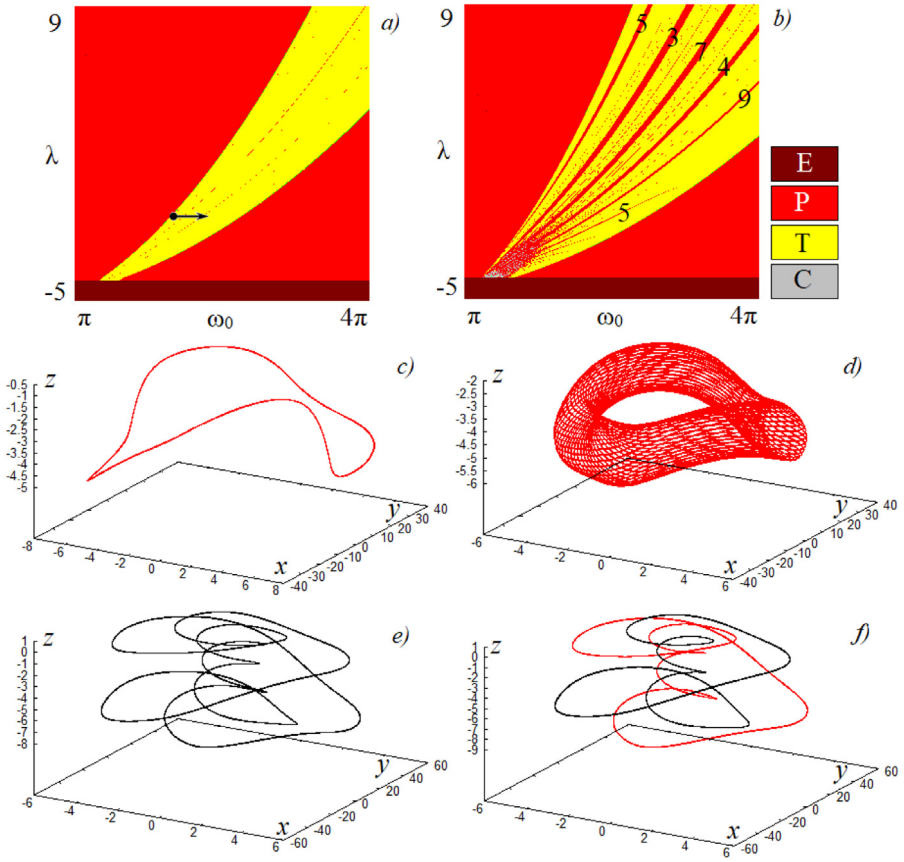

Fig. 1. Charts of Lyapunov exponents for the model generator of quasiperiodic oscillations (1), $\varepsilon = 4$, $b = 1$, $k = 0.02$. Parameters $\beta = 1/18$ (a) and $\beta = 1/25$ (b). In the legend E designates stable equilibrium state, P designates periodic oscillations, T relates to two-frequency quasiperiodic oscillations, and C to chaotic oscillations. The characteristic phase portraits of the model (1) for $\beta = 1/25$ and $\lambda = 1.4$, (c) $\omega_0 = \pi$, the base cycle of period-1; (d) $\omega_0 = 2\pi$, a torus; (e) $\omega_0 = 7.79$, the resonant cycle of period-7; (f) $\omega_0 = 8.64$, a pair of symmetric resonant cycles of period-4.

2π (the black point in Fig. 1a). Herewith, the frequency of the second generator is equal to $\omega_{02} = 2\pi + \Delta$. If $\lambda_2 = \lambda_1 = -1$ then, in accordance with Fig. 1a, variation of the frequency detuning Δ (the motion in the parameter plane along the horizontal line in the direction of the arrow in Fig. 1 a) in the region $\Delta > 0$ leaves predominantly the dynamics of the second generator quasiperiodic. When the value $\Delta_0 \approx 2.17$ is reached, the periodic regime corresponding to the basic limit cycle is realized. Thus, varying the frequency detuning, one can observe both a case of interaction of two generators in a quasiperiodic regime, and a case of a periodic regime in one of them.

Note that the picture depends on relation of the control parameters of the subsystems λ_1 and λ_2. We consider three cases: $\lambda_1 = \lambda_2$, $\lambda_1 < \lambda_2$ and $\lambda_1 > \lambda_2$, leaving the parameter of the first generator fixed.

To illustrate the dynamics of coupled generators, as the main tool we will use again the charts of Lyapunov exponents, like it was done for the individual autonomous generator. The legend establishing the correspondence between colors on the charts and the letter symbols is shown in Fig. 2 to the right. Classification of the regimes is explained in the Appendix.

Fig. 2 shows the charts of Lyapunov exponents in the parameter plane of the frequency detuning vs the coupling strength (Δ, M_C) for the system (4) at $\lambda_1 = -1$ and $\lambda_2 = -1, -0.5, -1.5$ (panels a, b, c, respectively). In the first chart (panel a), the arrow indicates the detuning value that corresponds to the transition of the second individual generator from the quasiperiodic regime to periodic self-oscillations in accordance with the chart of the individual generator of Fig. 1a.

Let us start the discussion with the case of a large coupling strength, $M_C > 3$ in Fig. 2a. In this case, as seen from Fig. 2a, with decrease of the frequency detuning Δ, three main types of regimes are observed: the stable equilibrium, the periodic regime, and the two-frequency quasiperiodic oscillations. Let us consider them in more detail.

Regime of oscillator death. Domain OD on the parameter plane (Δ, M_C) corresponds to stable equilibriums (2) in both generators. In accordance with the terminology [61], this is domain of the oscillator death (OD). As known, for two periodic oscillators, the oscillator death is observed at sufficiently large coupling strength and frequency detuning [61]. In our case, a similar situation occurs. However, now in the first generator in the case of absence of coupling we have the quasiperiodic oscillations. Taking into account also results from [61–63], we can deduce that effect of oscillator death shown here is a general feature for a wide class of oscillations in dynamical systems.

Complete Synchronization. Domain P on the parameter plane (Δ, M_C) having a tongue-like form corresponds to a regime of complete synchronization of two subsystems. Under complete synchronization we mean the transition to periodic oscillations determined as an exact coincidence of the points in the Poincaré section through each period. In accordance with [61], such transition is associated with suppression of the oscillations in the subsystems due to the strong coupling. The second generator without coupling could demonstrate here periodic or quasiperiodic regimes, but they are suppressed by the dissipative coupling.

Regime of Synchronous Quasiperiodicity. With decreasing frequency detuning Δ the system comes to a domain of two-frequency quasiperiodic oscillations (SC). In this case, the phases of the generators are mutually locked.

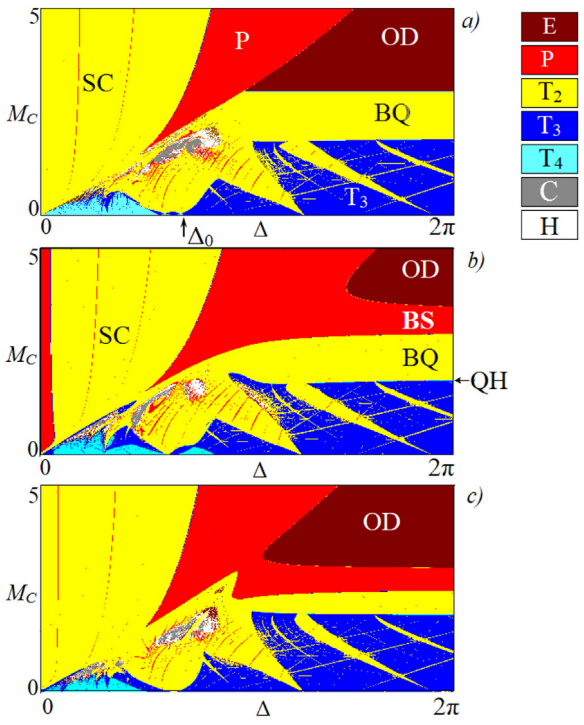

Fig. 2. Charts of Lyapunov exponents in the parameter plane (Δ, M_C) for coupled quasiperiodic generators (4) for $\varepsilon = 4$, $b = 1$, $k = 0.02$, $\beta = 1/18$. Values of control parameters are $\lambda_1 = -1$; (a) $\lambda_2 = -1$, (b) $\lambda_2 = -0.5$, (c) $\lambda_2 = -1.5$. OD is domain of oscillator death, P is periodic regime, SC is domain of synchronous quasiperiodicity, BQ is domain of broadband quasiperiodicity, BS is domain of broadband synchronization, QH is line of quasiperiodic Hopf bifurcation.

Fig. 3 a and b show examples of two phase portraits of generators in projections onto (x, y) and (x, z) planes in the regime of synchronous quasiperiodicity. Observe that the phase portraits of the first and the second generator look very similar, which is a consequence of the synchronization. In Fig. 3c time series for those attractors are shown. As one can see, time series relating to both subsystems are also very close. For both generators, the phase trajectories on the (x, y) plane do not visit a neighborhood of equilibrium in the origin. Thus, the phases of the generators can be well defined as

$$\varphi_i = \arctan(\frac{y_i}{x_i}). \tag{5}$$

In Fig. 3d and e the time dependence of the phase difference of the generators $(\varphi_1 - \varphi_2)$ and the phase diagram on the plane (φ_1, φ_2) are shown for this type of regime. These illustrations also demonstrate the phase synchronization of oscillations, which remain quasiperiodic.

For the coupled generators with well-defined phases, it is possible to determine the winding number w, as a ratio of the phase variation for projections of the phase trajectories on the plane (x, y) for each generator:

$$w = \lim_{t\to\infty} \frac{N_{x_1}}{N_{x_2}}, \tag{6}$$

where N_{x_1} and N_{x_2} are numbers of intersections of the hypersurfaces $x_1 = 0$ and $x_2 = 0$ by the phase trajectories, respectively. A calculation for the domain SC gives the value $w = 1$, which corresponds to exact synchronization of the phases of the generators. Thus, this regime can be called the synchronous quasiperiodicity (SC on the charts in Fig. 2). Note that for the domain of complete synchronization (P) the winding number is of the same value, $w = 1$.

Broadband Quasiperiodicity[2] and Broadband Synchronization. Let us decrease the value of the coupling parameter to $2 < M_C < 3$ and look at Fig. 2a. In this case, the synchronous quasiperiodicity and complete synchronization persist, but for large frequency detunings a new regime arises. In the parameter plane, it corresponds to a region of two-frequency quasiperiodicity. The respective domain in the parameter plane looks like a band of finite width in the coupling parameter and unbounded along the axis of frequency detuning. Such configuration allows us to interpret this domain as region of the broadband quasiperiodicity and denote it by BQ in Fig. 2.

In Fig. 2a, at decreasing coupling strength M_C, the two-frequency oscillations appear as an immediate behavior in the course of transition from the regime of oscillator death. There is certain degeneracy here (we discuss the corresponding bifurcations below). The degeneracy is removed as we set $\lambda_1 \neq \lambda_2$. This case is illustrated in Fig. 2b and c. One can see that between the regions of oscillator death (OD) and the broadband quasiperiodicity (BQ), a band of periodic regime appears adjacent to the complete synchronization tongue. Similar regimes were observed and described for coupled van der Pol oscillators non-identical in the control parameter [64]. In that case, the term broadband synchronization was proposed in [64]. The corresponding domain in Fig. 2b is marked as BS. By analogy with [65], the dynamical behavior in the BQ region adjacent to it can be defined as partial broadband synchronization.

Fig. 4 shows phase portraits observed as frequency detuning Δ increases as we move into the BQ region on the parameter plane for the case of identical oscillators. The phenomenon of broadband synchronization is associated with a difference in the dynamics of coupled subsystems. For instance, in the traditional system of coupled self-oscillators, a necessary condition for broadband synchronization is presence of the nonidentity in the excitation parameters of the oscillators [64]. For our system, we observe similar features. In the area of phase synchronization, or synchronous quasiperiodicity (SC), the attractors of each subsystem have the same size (we mean equal amplitude of oscillations for dynamical variables) (Fig. 3a). At the transition to the region of broadband quasiperiodicity, the oscillation amplitudes of the subsystems become different; this is most noticeable in the dynamics of the variables z_1 and z_2. With increasing frequency detuning, projection of the attractor of the second generator is compressed and tends to the equilibrium state, i.e. to the plane $(x_2, y_2, z_2) = (0, 0, \varepsilon)$. Furthermore, it can be seen that with increasing Δ, the phase trajectory of the first generator starts to visit a neighborhood of the origin, and the phase of the first generator becomes uncertain. Therefore, here we cannot speak of phase synchronization. At the same time, there are successive metamorphoses of tori, for example, appearance of a doubled torus (Fig. 4a, b) (below we describe it in detail, see Figs. 13–15 in Sect.4); emergence of a torus with a "band" structure (Fig. 4c); emergence of a so called multi-layered torus [66]. Note, a feature of Fig. 4: the first generator dominates under the second one, as can bee seen from the phase portraits. The dominance of one of the coupled subsystems is usually an attribute of the broadband synchronization regimes [64,65].

As broadband synchronization is associated with suppression of the own dynamics of one oscillator by another one, thus the study of the spectral characteristics of the subsystems and coupled systems is of interest. Fig. 5 presents the Fourier spectra for the first and the second subsystem (panels a and b, respectively)

[2] In order to escape misunderstanding we would like to emphasize, that in this case the term broadband quasiperiodicity is related to broadband synchronization in accordance to [54,55,64,65]. Regime of broadband quasiperiodicity does not mean quasiperiodic oscillations with broadband spectrum.

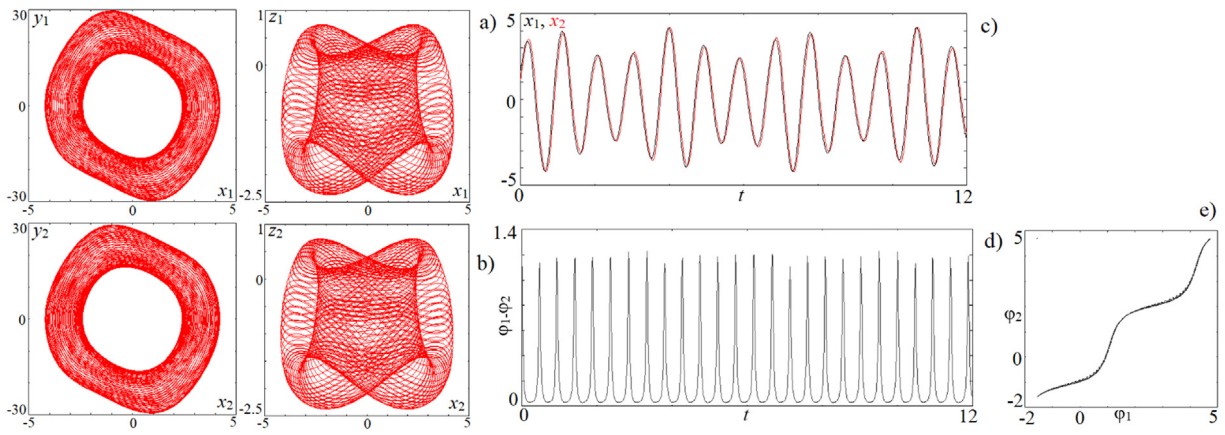

Fig. 3. Projections of the phase portrait of the first and second generators (a), (b); time series (c); dependence of the phase difference of the generators on time (d) and phase diagram (e) in the domain of synchronous quasiperiodicity. $\Delta = 0.5$, $M_C = 2.5$, $\varepsilon = 4$, $b = 1$, $k = 0.02$, $\lambda_1 = \lambda_2 = -1$, $\beta = 1/18$, $\omega_0 = 2\pi$.

and for coupled oscillators (panel c, black line is spectrum for x_1 variable, and red line is spectrum for x_2 variable). As seen from Fig. 5, the Fourier spectrum of the first oscillator has a typical form of two-frequency quasiperiodicity: it contains a main peak (in the vicinity of the frequency 1 Hz) and satellite peaks corresponding to the combination frequencies with the second frequency component. Fig. 5b shows the spectrum for the second subsystem; there is only one main peak strongly shifted towards higher frequencies, which corresponds to periodic self-oscillations. In Fourier spectra of both oscillators (Fig. 5c) the same frequency components present. In the spectrum for variable of the first generator x_1 the maximum is located in the vicinity of 1 Hz and it corresponds to the main peak of the first subsystem (Fig. 5a). The spectrum for the variable the second generator x_2 has maximum at frequency near the fundamental frequency of the second oscillator (Fig. 5b).

Arnold resonance web. At the decreasing coupling strength M_C in Fig. 2, a "web" is observed that is constituted by thin domains of two-frequency quasiperiodic regimes. At their intersection, islands of periodic regimes take place, and the whole structure is embedded in the region of three-frequency quasiperiodicity. Fig. 6 shows a zoomed fragment of the corresponding area in the parameter plane. Similar structures are characteristic for multifrequency regimes and are defined in [33,35] as the Arnold resonance web. It is clearly seen in Fig. 2a that such a picture arises when $\Delta > \Delta_0$, in the case of quasiperiodic oscillations in the first oscillator, and periodic oscillations in the second oscillator without coupling.

Tongues of quasiperiodic regimes with invariant tori of high dimension. At a small coupling strength in the region $\Delta < \Delta_0$, the four-frequency quasiperiodicity regime T_4 is observed, see Fig. 7. In this area three-frequency tongues are embedded; at a small coupling strength these tongues look similar to the traditional Arnold tongues.

In Fig. 7, one can see that for $\Delta > \Delta_0$ and for a small coupling strength regimes of the three-frequency quasiperiodicity T_3 are observed. The reason is simple: in accordance with Fig. 1a the second generator without coupling demonstrates periodic self-oscillations, the limit cycle.

Fig. 8 shows another zoomed fragment of the Lyapunov chart in the region to the left to the point Δ_0. It demonstrates two tongues of three-dimensional tori embedded into the domain of four-frequency quasiperiodicity. The tips of the tongues are located on the abscissa axis at points Δ_1 and Δ_2. As the coupling parameter increases, these tongues become wider and overlap, and the region of the overlap corresponds to occurrence of the two-frequency torus in a domain, which also has a tongue-like form. This tongue has a tip at the point Q, which corresponds to a certain threshold in terms of the coupling strength. The features of the picture from the point of view of quasiperiodic bifurcations will be discussed below.

4. Bifurcations of periodic and quasiperiodic regimes

Let us discuss several bifurcations, which are observed in the considered system. For model (1), as well as in other models with quasiperiodic dynamics, it is natural to analyze bifurcations of a steady state, limit cycles and tori attractors (quasiperiodic oscillations). For the two first ones bifurcation analysis is a standard procedure and can be performed with conventional software packages, for instance, XPP AUTO [67], and we will show these results in the next subsection. Bifurcation analysis of quasiperiodic oscillations is not trivial procedure. In accordance with [33,68,69] three types of quasiperiodic bifurcations can be distinguished: (i) quasiperiodic Hopf bifurcation; (ii) saddle–node quasiperiodic bifurcation; (iii) quasiperiodic period-doubling bifurcation. The last is also called a bifurcation of torus doubling. Further we will consider all these cases. Methods, which we will use for bifurcational analysis are described in the Appendix.

Regime of complete synchronization. In Fig. 9 bifurcation lines, bounding a domain of complete synchronization, are shown. These lines were obtained using software package of numerical bifurcation analysis XPP AUTO [67]. In Fig. 9 the lines of Neimark–Sacker bifurcations are depicted by green lines (NS) and the lines of Andronov–Hopf bifurcations are shown by blue lines (AH).

For all three cases of Fig. 9, the left boundary of the tongue of complete synchronization corresponds to the Neimark–Sacker bifurcation, as a result of which the limit cycle becomes unstable, and a two-frequency torus appears. In the case of identical control parameters (Fig. 9a) the right boundary of the tongue for a small coupling strength is also a Neimark–Sacker bifurcation line. This line ends at the point p_2 (3.034, 2.978) on the parameter plane (Δ, M_C), coming to the line of Andronov–Hopf bifurcation at $M_C = 3$. For large values of the coupling strength, the boundary of the complete synchronization tongue is the Andronov–Hopf bifurcation, as a result of which the equilibrium state loses stability, and a stable limit cycle appears.

As discussed in Section 3, the case of identical parameters λ is a kind of degeneracy. In this case, the Andronov–Hopf bifurcation line bumps into the Neimark–Sacker bifurcation line at the point p_2, forming a sharp angle. The condition of Andronov–Hopf bifurcation in each oscillator without coupling is given by Eq. (3). The term responsible for the coupling of the oscillators also introduces dissipation in the system. In the case of identical parameters

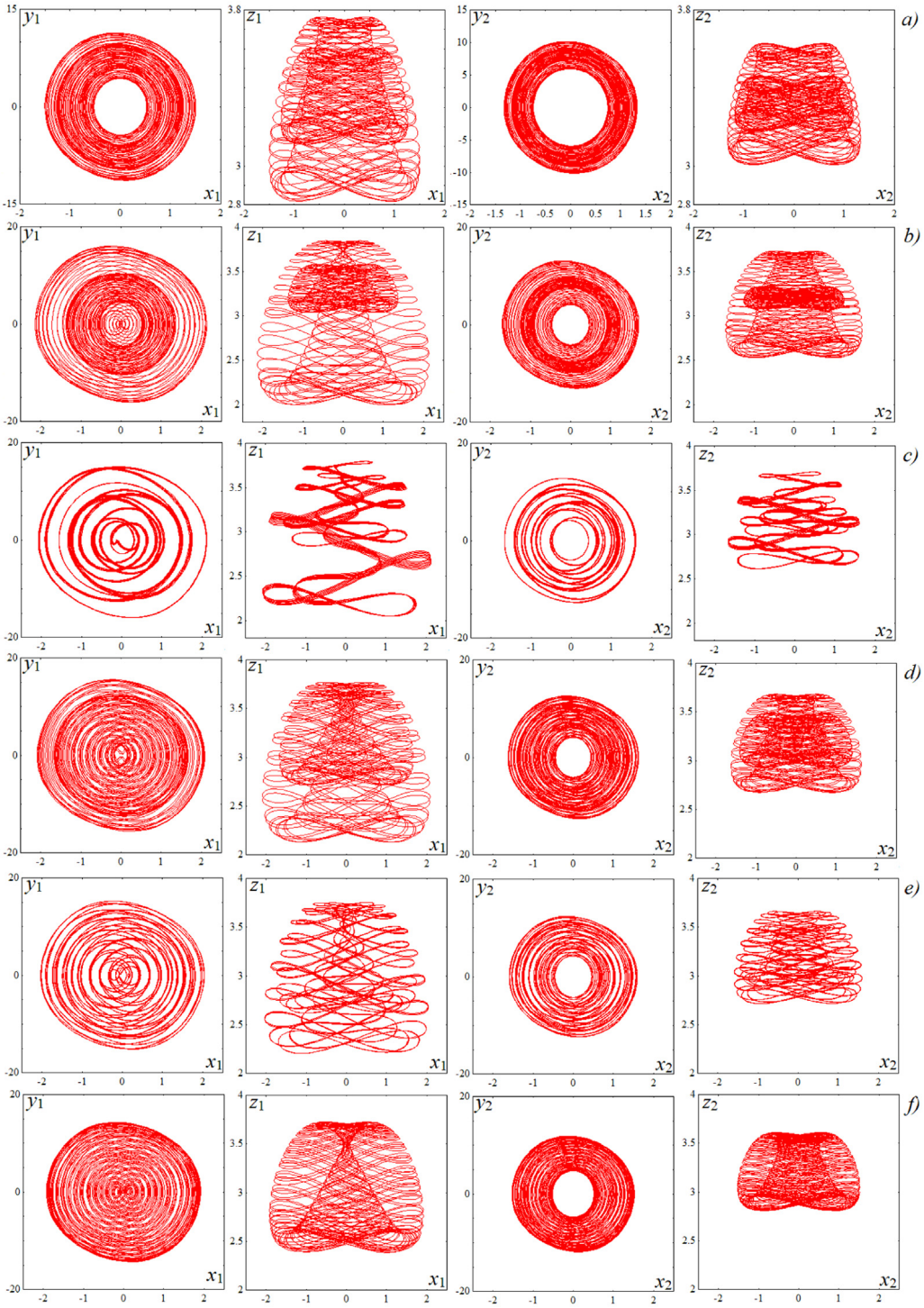

Fig. 4. Phase portraits of two generators in the region of the broadband quasiperiodicity; $M_C = 2.5$, $\varepsilon = 4$, $b = 1$, $k = 0.02$, $\lambda_1 = \lambda_2 = -1$, $\beta = 1/18$, $\omega_0 = 2\pi$; (a) $\Delta = 2.58$; (b) $\Delta = 2.7$; (c) $\Delta = 2.76$; (d) $\Delta = 2.78$; (e) $\Delta = 2.79$; (f) $\Delta = 2.81$.

λ, the stabilization of equilibria in the subsystems occurs simultaneously. Thus, the lower boundary of the Andronov–Hopf bifurcation line is determined by the equation $M_C^{OD} = \varepsilon + \lambda = 3$, which is in a good agreement with the charts of Lyapunov exponents. When the coupling strength is less than M^{OD} a two-frequency torus occurs for the identical oscillators. Fig. 10 shows the dependence of the largest four Lyapunov exponents on the coupling parameter; one can see in this case for $M_C < 3$ that all four exponents are negative. At the Andronov–Hopf bifurcation, the largest four exponents become zero, it means that there is a degeneration of the bifurcation. In Figs. 9a and 10, the degenerate Andronov–Hopf bifurcation is denoted as dAH. With further decrease of the parameter, the largest two exponents remain zero, while the other two become negative.

In Fig. 9b and c the bifurcation lines are shown also for the cases of non-identical parameters λ, i.e. when the degeneracy is removed. In the case when $\lambda_1 < \lambda_2$ there are two bifurcation lines on the parameter plane (Fig. 9b): the Andronov–Hopf bifurcation line (AH) and the Neimark–Sacker bifurcation line (NS). In this case, the Andronov–Hopf bifurcation line is continuous and

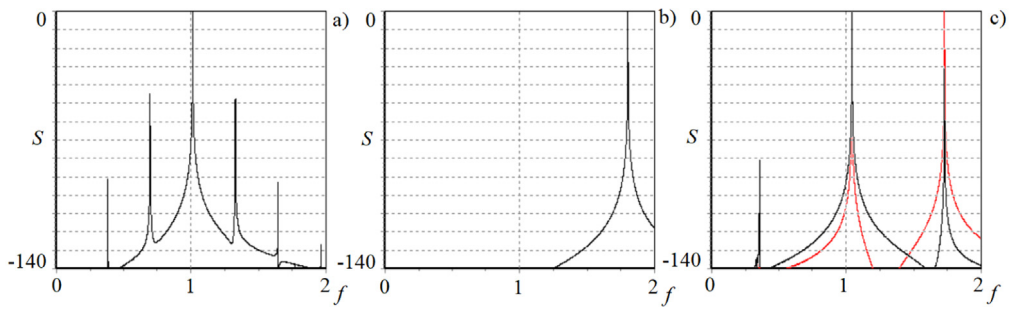

Fig. 5. Fourier spectrums of the first (a), the second subsystems (b) and coupled generators (c) in the region of the broadband quasiperiodicity (black line is spectrum for x_1 variable, and red line is spectrum for x_2 variable); $\varepsilon = 4$, $b = 1$, $k = 0.02$, $\lambda_1 = \lambda_2 = -1$, $\beta = 1/18$; (a) $\omega_0 = 2\pi$; (b) $\omega_0 = 2\pi + 5$; (c) $\omega_0 = 2\pi$, $\Delta = 5$, $M_C = 2.5$. (For interpretation of the references to color in this figure legend, the reader is referred to the web version of this article.)

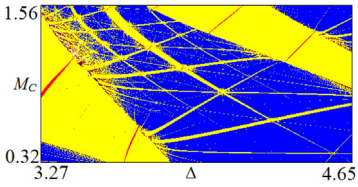

Fig. 6. Zoomed fragment of Fig. 2a corresponding to the Arnold resonance web on the basis of a three-dimensional torus. $\varepsilon = 4$, $b = 1$, $k = 0.02$, $\lambda_1 = \lambda_2 = -1$, $\beta = 1/18$, $\omega_0 = 2\pi$.

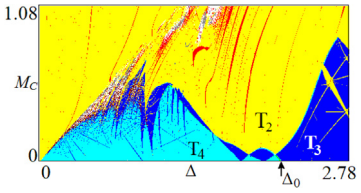

Fig. 7. Zoomed fragment of Fig. 2a. The interval of the frequency detuning corresponds to the transition of the second generator to the regime of the basic limit cycle; $\varepsilon = 4$, $b = 1$, $k = 0.02$, $\lambda_1 = \lambda_2 = -1$, $\beta = 1/18$, $\omega_0 = 2\pi$.

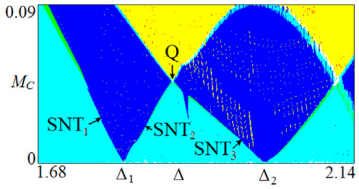

Fig. 8. Zoomed fragment of Fig. 7. SNT are the lines of saddle–node bifurcations of invariant tori, and Q is the point of a quasiperiodic bifurcation of codimension two; $\varepsilon = 4$, $b = 1$, $k = 0.02$, $\lambda_1 = \lambda_2 = -1$, $\beta = 1/18$, $\omega_0 = 2\pi$.

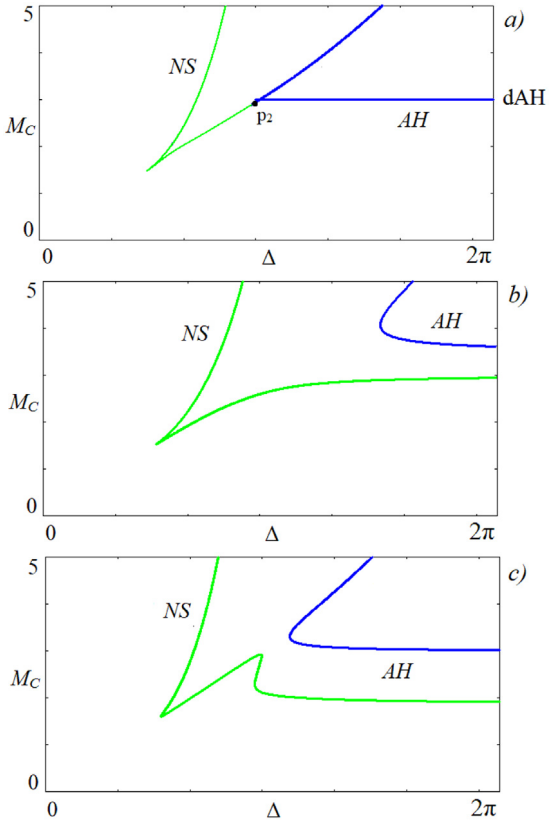

Fig. 9. The bifurcation lines associated with the domain of complete synchronization, the parameters correspond to Fig. 2. NS is Neimark–Sacker bifurcation, LP is saddle–node bifurcation, AH is Andronov–Hopf bifurcation, dAH is degenerate Andronov–Hopf bifurcation.

smooth, been located above the Neimark–Sacker bifurcation line, and they do not intersect, forming the broadband synchronization domain (Fig. 2b).

For $\lambda_1 > \lambda_2$ the picture of the bifurcation lines slightly changes (Fig. 9c). The shape of the Andronov–Hopf bifurcation line remains unchanged. The Neimark–Sacker bifurcation line acquires an additional inflection as the frequency detuning increases; a broadband synchronization domain is also formed.

If the parameters λ_1 and λ_2 are non-identical, then each oscillator has its own threshold of equilibrium stabilization, in our cases for the first oscillator it is always $M^{OD} = 3$, but for the second oscillator it will be different: for $\lambda_2 = -1.5$, $M^{OD} = 3.5$, and for $\lambda_2 = -0.5$, $M^{OD} = 2.5$. In the case when the second oscillator requires a large coupling strength to stabilize the equilibrium ($\lambda_2 = -1.5$, Fig. 9b), at the moment of the equilibrium stabilization in the first oscillator ($M_C = 3$), the system shows

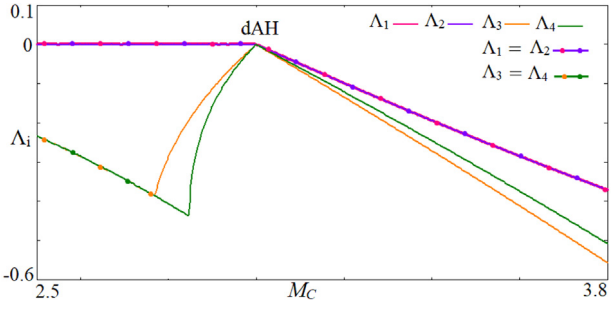

Fig. 10. Dependence of the largest four Lyapunov exponents on the coupling strength, illustrating the degenerate Andronov–Hopf bifurcation dAH. The case of equal parameters λ. Other parameters are $\Delta = 2\pi$, $\varepsilon = 4$, $b = 1$, $k = 0.02$, $\lambda_1 = \lambda_2 = -1$, $\beta = 1/18$, $\omega_0 = 2\pi$.

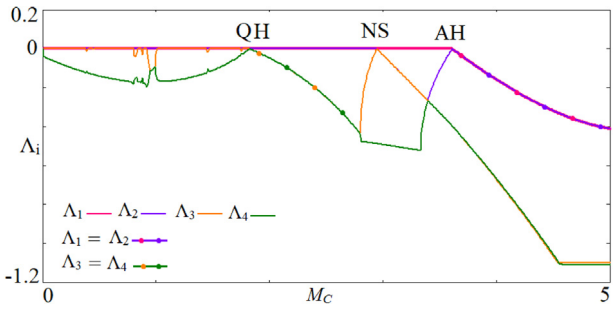

Fig. 11. Dependence of the largest four Lyapunov exponents on the coupling strength; $\Delta = 2\pi$, $\varepsilon = 4$, $b = 1$, $k = 0.02$, $\beta = 1/18$, $\omega_0 = 2\pi$, $\lambda_1 = -1$, $\lambda_2 = -0.5$. AH is the Andronov–Hopf bifurcation, NS is the Neimark–Sacker bifurcation, and QH is the quasiperiodic Hopf bifurcation.

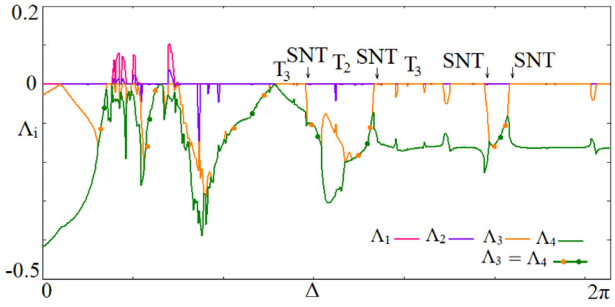

Fig. 12. Dependence of the largest four Lyapunov exponents on the frequency detuning; $\varepsilon = 4$, $b = 1$, $k = 0.02$, $\beta = 1/18$, $\omega_0 = 2\pi$, $\lambda_1 = -1$, $\lambda_2 = -0.5$; $M_C = 0.72$. SNT are the points of saddle–node quasiperiodic bifurcations of tori.

appearance of complete synchronization and of periodic oscillations. With further increase of the coupling strength, and reaching the threshold of equilibrium stabilization in the second oscillator ($M^{OD} = 3.5$), the equilibrium is stabilized in the whole system of coupled oscillators. In the case when the second oscillator requires smaller coupling strength to stabilize the equilibrium ($\lambda_2 = -0.5$, Fig. 9c), the equilibrium stabilization in the system of coupled oscillators also occurs when both oscillators reach the thresholds, and in this case the threshold is $M_C = 3$.

Quasiperiodic Hopf bifurcation. The domains of quasiperiodic oscillations in the parameter plane are bounded by the lines of quasiperiodic bifurcations. Let us analyze the quasiperiodic bifurcations using rigorous approach basing on Lyapunov exponents [33]; details of the method see in the Appendix.

Fig. 11 shows the plots of the largest four Lyapunov exponents as functions of the coupling parameter, depicted for a large value of the frequency detuning $\Delta = 2\pi$ that corresponds to the right edge of the chart in Fig. 2b. This is the case of non-identical control parameters λ_1, λ_2. One can see that the point of degenerate bifurcation (dAH) in Fig. 10 splits into the Andronov–Hopf bifurcation (AH) and the Neimark–Sacker bifurcation (NS). Thus, in this case the degeneration is removed.

As the coupling parameter decreases, the quasiperiodic Hopf bifurcation of the two-dimensional torus occurs. In this case, below the bifurcation point, two Lyapunov exponents coincide: $\Lambda_3 = \Lambda_4$. At the bifurcation point, one of them vanishes $\Lambda_3 = 0$, and another Λ_4 becomes negative, this is a quasiperiodic Hopf bifurcation. Thus, quasiperiodic Hopf bifurcation bounds the domain of broadband quasiperiodicity, which is marked by an arrow with the symbol QH on the chart of Fig. 2b.

Saddle–node bifurcations of tori. Fig. 12 shows illustrations for the dependence of the Lyapunov exponents on the frequency detuning in the domain of a small fixed coupling parameter

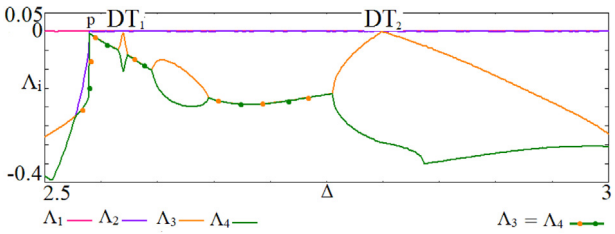

Fig. 13. Dependence of the largest four Lyapunov exponents when moving on the parameter plane to the domain of broadband quasiperiodicity with marked points of the tori doubling bifurcations, DT; $\varepsilon = 4$, $b = 1$, $k = 0.02$, $\beta = 1/18$, $\omega_0 = 2\pi$, $\lambda_1 = -1$, $\lambda_2 = -1$; $M_C = 2.5$.

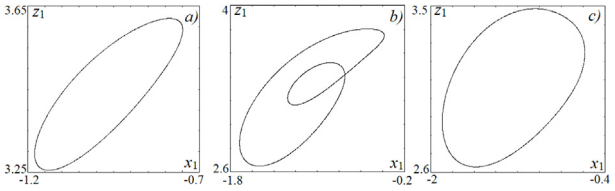

Fig. 14. Poincaré sections illustrating the tori doubling bifurcations; $\varepsilon = 4$, $b = 1$, $k = 0.02$, $\beta = 1/18$, $\omega_0 = 2\pi$, $\lambda_1 = -1$, $\lambda_2 = -1$; $M_C = 2.5$; (a) $\Delta = 2.55$; (b) $\Delta = 2.6$; (c) $\Delta = 3.14$.

$M_C = 0.72$. The chosen road in Fig. 2b intersects the domain of three-frequency quasiperiodicity and the embedded tongues of two-dimensional tori. As seen from the plots of Lyapunov exponents, the boundaries of these tongues are formed by the lines of saddle–node bifurcations of invariant tori SNT, when one of the Lyapunov exponents Λ_3 becomes zero, and, so, it remains inside the domain of three-frequency quasiperiodicity [33]. Arrows in the figure show these boundaries for two regions of two-dimensional tori. In fact, there are more of them; the corresponding resonance windows are clearly visible in Fig. 12.

Saddle–node bifurcations of tori SNT on the basis of tori of higher dimension form the boundaries of the tongues of three-dimensional tori in the region $\Delta < \Delta_0$, as shown in Fig. 8. It is easy to see that the point Q in Fig. 8 corresponds to intersection of two lines of saddle–node bifurcations of tori SNT_2 and SNT_3, which relate to two different tongues. Thus, the edge of the domain of the two-dimensional torus Q can be interpreted as a quasiperiodic bifurcation of codimension two.

Bifurcation of torus doubling. When moving to the area of broadband quasiperiodicity in the parameter plane, a torus doubling bifurcation is observed. The points of such bifurcation DT in accordance with the rules [33] are identified from the plots of Lyapunov exponents in Fig. 13. The values of the frequency detuning corresponding to the torus doubling are approximately $\Delta \approx 2.57$ and $\Delta \approx 2.8$. The doubling of the torus is diagnosed reliably from the portraits of attractors in the Poincaré section shown in Fig. 14. In this case, the Poincaré section is obtained as a two-dimensional projection onto the plane of the variables of the first oscillator (x_1, z_1) for a fixed variable $y_1 = 0$. Fig. 14 shows that the point DT_1 corresponds to the doubling of the original torus, and the point DT_2 corresponds to the "inverse" bifurcation, when the doubled torus transforms topologically into the original torus.

The tori doublings are also diagnosed from the bifurcation trees, see Fig. 15a. Note that on the enlarged fragment of the bifurcation tree in Fig. 15b the windows corresponding to appearance of the multi-layered tori are well seen, like those shown in Fig. 4c, e.

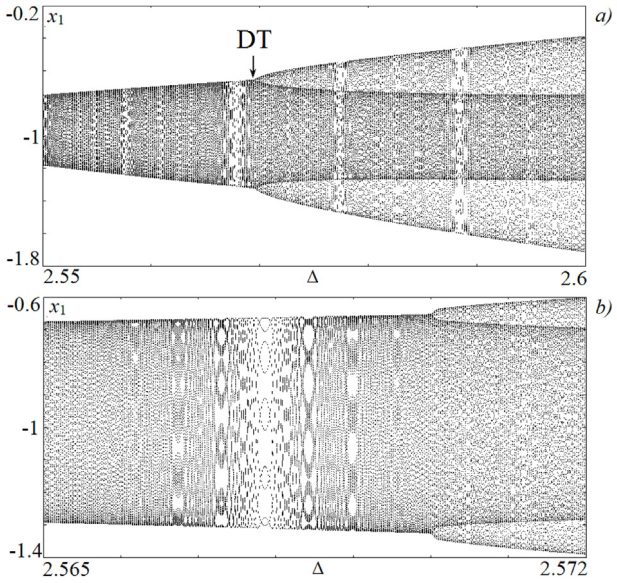

Fig. 15. Bifurcation trees demonstrating the torus doubling and the appearance of multi-layered tori; $\varepsilon = 4$, $b = 1$, $k = 0.02$, $\beta = 1/18$, $\omega_0 = 2\pi$, $\lambda_1 = -1$, $\lambda_2 = -1$; $M_C = 2.5$.

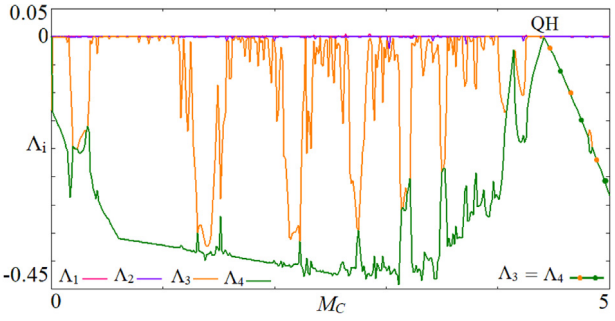

Fig. 17. Dependence of the largest four Lyapunov exponents, corresponding to the chart in Fig. 16a and $\Delta = 4\pi$.

5. Parameter plane arrangement for another choice of parameters

Let us now discuss another choice of the parameters of the individual generators, corresponding to Fig. 1b. As it was noted above, this case corresponds to a possibility of pronounced periodic resonances inside the domain of quasiperiodicity. Let us turn to the chart of Lyapunov exponents of the coupled generators shown in Fig. 16. The color palette here is identical to that of Fig. 2. But there appear regions of new type, which correspond to chaos with one positive and two zero Lyapunov exponents. In Fig. 16, in addition to the palette of Fig. 2, these domains are shown in black.

A number of other differences also can be specified. In the domain of the Arnold resonance web, zones of two-dimensional tori transform into horizontal bands, analogous to the domain of the broadband quasiperiodicity. The dependence of the largest four Lyapunov exponents on the coupling parameter along the right edge of the chart is shown in Fig. 17. The boundaries of the domains of the two-frequency quasiperiodicity correspond to the saddle–node bifurcations of invariant tori.

A vicinity of the point Δ_0 corresponding to the transition of the second generator to the regime of the limit cycle is shown in Fig. 16d. When $\Delta < \Delta_0$, there is a set of tongues of two-dimensional tori embedded in the domain of three-dimensional tori. It is interesting that the picture looks similar to the traditional Arnold tongues, but now it is for the invariant tori. Inside these tongues, there are several doublings of the basic torus, followed by its destruction and transition to chaos. As seen from

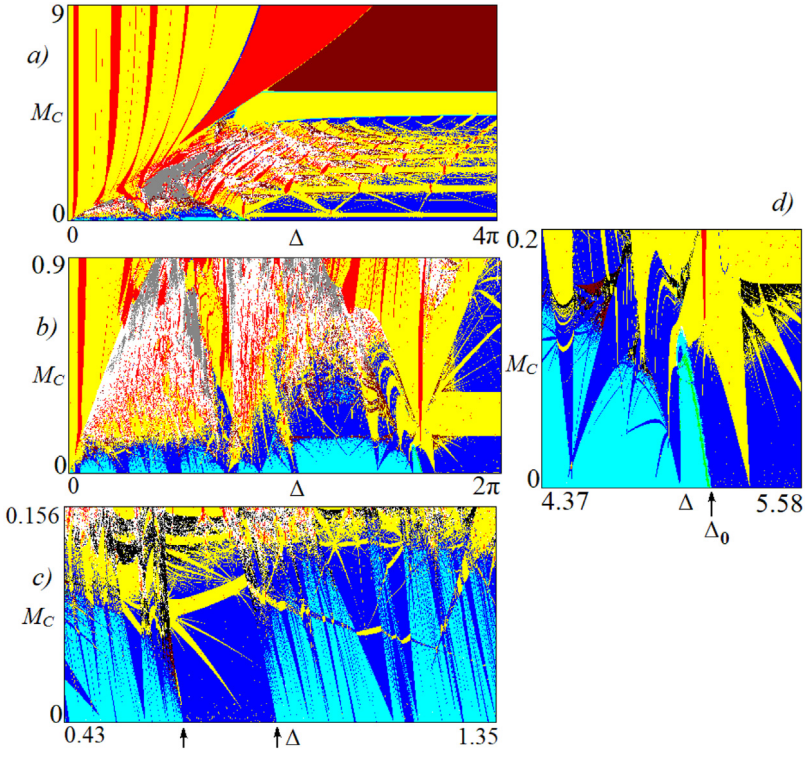

Fig. 16. Chart of Lyapunov exponents (a) and its zoomed fragment (b, c, d). $\varepsilon = 4$, $b = 1$, $k = 0.02$, $\beta = 1/25$, $\omega_0 = 2\pi$, $\lambda_1 = 1.4$, $\lambda_2 = 1.4$.

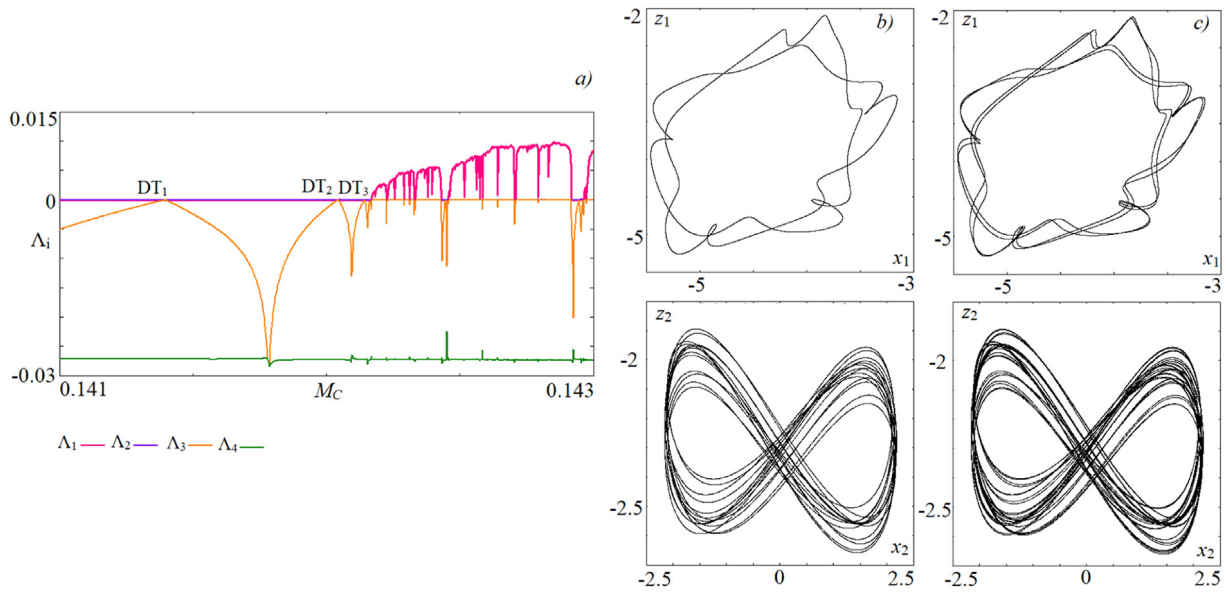

Fig. 18. (a) Dependence of the largest four Lyapunov exponents corresponding to the chart in Fig. 16d at $\Delta = 5.3743$. (b, c) Evolution of a two-dimensional torus in the Poincaré section when moving within the corresponding tongue in Fig. 16d. Here $\varepsilon = 4$, $b = 1$, $k = 0.02$, $\beta = 1/25$, $\omega_0 = 2\pi$, $\lambda_1 = 1.4$, $\lambda_2 = 1.4$, $\Delta = 5.3743$; (b) $M_C = 0.141$; (c) $M_C = 0.1415$.

Fig. 16d, outside the tongues the chaotic regime arises with two zero Lyapunov exponents.[3]

Fig. 18a shows a graph of the Lyapunov exponents versus the coupling parameter in the transition from the central tongue of the two-frequency quasiperiodicity to chaos with two zero Lyapunov exponents. In the transition, three bifurcations of torus doubling, DT_1, DT_2, DT_3 are well seen, after which the largest exponent Λ_1 becomes positive, and the next two Λ_2 and Λ_3 vanish. Formation of such kind of chaotic attractors was noted for maps in [70,71]. Fig. 18b and c show Poincaré sections by the hypersurface $y_1 = 0$ in the projections onto the planes of variables of the first and second generators just before and after the torus doubling bifurcation. In the projection onto the plane of the variables of the first generator, the invariant curve has a complex structure, with six characteristic breaks and self-intersections. The picture in Poincaré section in projection onto the plane of the second oscillator differs greatly from the first one, and has a figure-eight shape with twelve loops. Despite the fact that the invariant curve has such a complex shape, the bifurcation of the torus doubling can be clearly seen in (Fig. 18c).

At $\Delta < \Delta_0$ narrow tongues of three-dimensional tori embedded in the domain of four-dimensional tori are observed. In this case the structure of the tongues differs from the traditional one, see Fig. 16c. In this figure, one can observe two types of domains of resonant three-dimensional tori, tongues of traditional type with narrow tips, as well as domains that have a pedestal of finite width. The most significant formation of this kind is indicated by two arrows in Fig. 16c. The reason for appearance of such formations was explained in our discussion of Fig. 1b. In this case, when the frequency of the second generator (i.e., frequency detuning) varies, the subsystem hits into the resonant domains of the periodic regime, which provides a finite width of the base of the domain of three-frequency tori for the coupled generators. (Remind that the first generator operates in the regime of two-frequency quasiperiodicity.)

With growth of the coupling parameter in Fig. 16c, one can see a nontrivial internal structure of the domains of three-frequency tori. Fan-shaped structures of two-dimensional torus regions are observed with inclusions of chaos regions.

6. Conclusion

Features of mutual synchronization of quasiperiodic oscillations are investigated for a model example of two coupled quasiperiodic oscillators with an equilibrium state. The structure of the parameter plane (frequency detuning vs coupling strength) was studied. It is shown that in such a system the domains of oscillator death, periodic regimes (complete synchronization), phase synchronization of quasiperiodic oscillations, broadband synchronization, Arnold resonance web formations occur. Illustrations of each type of the regimes and the bifurcations associated with them are given. In particular, bifurcations of invariant tori were observed: a quasiperiodic Hopf bifurcation, saddle–node bifurcations of tori, doubling of invariant tori, and bifurcations of codimension two. A change in the parameter plane structure is shown, when one of the interacting generators passes from the regime of quasiperiodic oscillations to the region of the basic limit cycle. The cases of predominantly quasiperiodic regimes and the case of embedded resonances for the second generator are considered separately. Several types of domains of invariant tori of different dimensions and their internal structures are described. Results of the conducted investigations indicate richness and diversity of phenomena intrinsic to the problem of interaction (synchronization) of the quasiperiodic oscillators.

Acknowledgment

The work was carried out with the financial support of the Russian Science Foundation, grant No. 17-12-01008.

Appendix. Methods of investigation

Unfortunately, at the present moment there are no adequate methods for analyzing quasiperiodic bifurcations, developed up to a comparable degree as those for bifurcations of periodic regimes. In the present paper we use the following approaches: (i) analysis of the full spectrum of Lyapunov exponents, method

[3] We have to remark that for this case zero Lyapunov exponents are not exactly zero, but very close, for our numerical computations we get the accuracy about 10^{-5}.

of charts of Lyapunov exponents; (ii) bifurcational analysis for equilibrium states and periodic oscillations; and (iii) rigorous bifurcational analysis of quasiperiodic oscillations based on consideration of behavior of the Lyapunov exponents near a bifurcation point. Let us shortly describe all these techniques.

To depict a chart of Lyapunov exponents, for each pixel of the parameter plane area the full spectrum of Lyapunov exponents is calculated. For calculating the Lyapunov exponents we use well-known Benettin algorithm with Gram–Schmidt orthogonalization of the perturbation vectors [72,73]. It is clear that the Lyapunov exponents are averaged characteristics; their numerically obtained values depend to some extent on the length of time series and time intervals between normalization of the perturbation vectors. In our computational procedures we determine optimal parameters, the compromise between accuracy and time for calculating. Then we chose a threshold *Thr*, which was used to diagnose for zero Lyapunov exponents. In the most of our numerical experiments we set $Thr = 0.0001$. Thus, we distinguish the next options: (i) $\Lambda_i > Thr$ that corresponds to a positive Lyapunov exponents; (ii) if $|\Lambda_i| < Thr$, then we suggest that the Lyapunov exponent is zero; and (iii) $\Lambda_i < -Thr$ that corresponds to a negative Lyapunov exponent. The number of Lyapunov exponents and variety of dynamical regimes depend on the dimension of considering model.

In the frame of this work we deal with three-dimensional and six-dimensional systems.

In accordance with the signature of the spectrum of Lyapunov exponents, the pixels on the parameter plane of three-dimensional model was colored in accordance with the accepted legend:

(1) E means stable equilibrium point, $\Lambda_1 < 0$, $\Lambda_2 < 0$, $\Lambda_3 < 0$;
(2) P means periodic oscillations (limit cycle), $\Lambda_1 = 0$, $\Lambda_2 < 0$, $\Lambda_3 < 0$;
(3) T means two-frequency quasiperiodic oscillations, $\Lambda_1 = 0$, $\Lambda_2 = 0$, $\Lambda_3 < 0$;
(4) C means chaotic oscillations, $\Lambda_1 > 0$, $\Lambda_2 = 0$, $\Lambda_3 < 0$.

In the case of six-dimensional dynamical systems the analysis is performed considering six Lyapunov exponents using the following notations:

(1) E designates occurrence of stable equilibrium point, $\Lambda_1 < 0$, $\Lambda_2 < 0$, $\Lambda_3 < 0$, $\Lambda_4 < 0$, $\Lambda_5 < 0$, $\Lambda_6 < 0$;
(2) P designates periodic oscillations (limit cycles), $\Lambda_1 = 0$, $\Lambda_2 < 0$, $\Lambda_3 < 0$, $\Lambda_4 < 0$, $\Lambda_5 < 0$, $\Lambda_6 < 0$;
(3) T_2 relates to two-frequency quasiperiodic oscillations, $\Lambda_1 = 0$, $\Lambda_2 = 0$, $\Lambda_3 < 0$, $\Lambda_4 < 0$, $\Lambda_5 < 0$, $\Lambda_6 < 0$;
(4) T_3 corresponds to three-frequency quasiperiodic oscillations, $\Lambda_1 = 0$, $\Lambda_2 = 0$, $\Lambda_3 = 0$, $\Lambda_4 < 0$, $\Lambda_5 < 0$, $\Lambda_6 < 0$;
(5) T_4 relates to four-frequency quasiperiodic oscillations, $\Lambda_1 = 0$, $\Lambda_2 = 0$, $\Lambda_3 = 0$, $\Lambda_4 = 0$, $\Lambda_5 < 0$, $\Lambda_6 < 0$;
(6) C designates chaotic oscillations, $\Lambda_1 > 0$, $\Lambda_2 = 0$, $\Lambda_3 < 0$, $\Lambda_4 < 0$, $\Lambda_5 < 0$, $\Lambda_6 < 0$;
(7) HC corresponds to hyperchaos, $\Lambda_1 > 0$, $\Lambda_2 > 0$, $\Lambda_3 = 0$, $\Lambda_4 < 0$, $\Lambda_5 < 0$, $\Lambda_6 < 0$.

The second approach, which we use in this paper, is analysis of bifurcations of equilibrium point and periodic cycles. For this analysis we exploit a special software package XPPAUTO [67]. It allows determining main bifurcations of equilibrium points and limit cycles with analysis of multipliers, which are determined by numerically-analytic methods, details see in [67].

The third approach is a rigorous bifurcation analysis of tori suggested in [33]. In accordance with [33], analyzing behavior of the Lyapunov exponents near a bifurcation point one can distinguish three quasiperiodic bifurcations:

(i) Quasiperiodic Hopf bifurcation: before the bifurcation point, two maximal negative Lyapunov exponents coincide: $\Lambda_n = \Lambda_{n+1}$. At the bifurcation point, both of them touch zero axis, then one of them vanishes: $\Lambda_n = 0$, and the other Λ_{n+1} becomes negative.

(ii) Saddle–node quasiperiodic bifurcations: before the bifurcation point, two negative Lyapunov exponents after zero are not the same, Λ_n and Λ_{n+1}. At the bifurcation point, one of them vanishes: $\Lambda_n = 0$, and the other Λ_{n+1} remains negative, and does not touch zero.

(iii) Period-doubling of torus: before the bifurcation point, two negative Lyapunov exponents after zero are not the same, Λ_n and Λ_{n+1}. At the bifurcation point, one of them touches zero: $\Lambda_n = 0$, and the other Λ_{n+1} remains negative.

References

[1] G. Chen, T. Ueta, Chaos in Circuits and Systems, World Scientific, 2002.
[2] F.C. Moon, Chaotic and Fractal Dynamics: Introduction for Applied Scientists and Engineers, John Wiley & Sons, 2008.
[3] B. Muthuswamy, L.O. Chua, Simplest chaotic circuit, Int. J. Bifur. Chaos 20 (05) (2010) 1567–1580.
[4] V.S. Anishchenko, Dynamical Chaos: Models and Experiments, World Scientific, Singapore, 1995.
[5] J.C. Sprott, Elegant Chaos: Algebraically Simple Chaotic Flows, World Scientific, 2010.
[6] A.S. Dmitriev, E.V. Efremova, N.A. Maksimov, A.I. Panas, Generation of Chaos, Technosfera, Moscow, 2012 (in Russian).
[7] A.S. Dmitriev, A.I. Panas, Dynamic Chaos: New Information Carriers for Communications Systems, Fizmatlit, Moscow, 2002 (in Russian).
[8] E.A. Myasin, Investigations of the hf noise generation in IRE of Academy of Sciences of USSR at 1962–1967 years - The beginning of the new science direction, Izv. Vyssh. Uchebn. Zaved. Appl. Nonlinear Dyn. 22 (1) (2014) 104–122 (in Russian).
[9] K.A. Lukin, Noise radar technology, Telecommun. Radio Eng. 55 (12) (2001) 8–16.
[10] T. Stojanovski, L. Kocarev, Chaos-based random number generators-part I: analysis, IEEE Trans. Circuits Syst. I 48 (3) (2001) 281–288.
[11] T. Stojanovski, J. Pihl, L. Kocarev, Chaos-based random number generators. Part II: practical realization, IEEE Trans. Circuits Syst. I 48 (3) (2001) 382–385.
[12] M.S. Baptista, Cryptography with chaos, Phys. Lett. A 240 (1–2) (1998) 50–54.
[13] M.P. Kennedy, Chaos in the Colpitts oscillator, IEEE Trans. Circuits Syst. I 41 (11) (1994) 771–774.
[14] P. Kvarda, Chaos in Hartley's oscillator, Int. J. Bifurcation Chaos 12 (10) (2002) 2229–2232.
[15] L. Keuninckx, G. Van der Sande, J. Danckaert, Simple two-transistor single-supply resistor-capacitor chaotic oscillator, IEEE Trans. Circuits Syst. II 62 (9) (2015) 891–895.
[16] L.O. Chua, C.W. Wu, A. Huang, G.Q. Zhong, A universal circuit for studying and generating chaos. I. Routes to chaos, IEEE Trans. Circuits Syst. I 40 (10) (1993) 732–744.
[17] M.P. Kennedy, Robust op amp realization of Chua's circuit, Frequenz. J. RF-Eng. Telecommun. 46 (3–4) (1992) 66–80.
[18] O. Morgul, Wien bridge based RC chaos generator, Electron. Lett. 31 (24) (1995) 2058–2059.
[19] E.V. Efremova, A.S. Dmitriev, Ultrawideband microwave 3-7 ghz chaotic oscillator implemented as sige integrated circuit, in: Springer Proceedings in Physics, vol. 191, 2017, pp. 71–80.
[20] J. Kengne, N. Tsafack, L.K. Kengne, Dynamical analysis of a novel single Opamp-based autonomous LC oscillator: antimonotonicity, chaos, and multiple attractors, Int. J. Dyn. Control (2018) 1–15.
[21] R. Tchitnga, et al., Chaos in a single op-amp-based jerk circuit: Experiments and simulations, IEEE Trans. Circuits Syst. II 63 (3) (2016) 239–243.
[22] J. Kengne, A.N. Negou, D. Tchiotsop, Antimonotonicity, chaos and multiple attractors in a novel autonomous memristor-based jerk circuit, Nonlinear Dynam. 88 (4) (2017) 2589–2608.
[23] T. Matsumoto, Chaos in electronic circuits, Proc. IEEE 75 (8) (1987) 1033–1057.
[24] S. Wieczorek, B. Krauskopf, D. Lenstra, Mechanisms for multistability in a semiconductor laser with optical injection, Opt. Commun. 183 (2000) 215–226.
[25] Y. Nishiuchi, T. Ueta, H. Kawakami, Stable torus and its bifurcation phenomena ia a three-dimensional autonomous circuit, Chaos Solitons Fractals 27 (2006) 941–951.
[26] V. Anishchenko, S. Nikolaev, Generator of quasi-periodic oscillations featuring two-dimensional torus doubling bifurcations, Tech. Phys. Lett. 31 (10) (2005) 853–855.

[27] A.P. Kuznetsov, S.P. Kuznetsov, N.V. Stankevich, A simple autonomous quasiperiodic self-oscillator, Commun. Nonlinear Sci. Numer. Simul. 15 (6) (2010) 1676–1681.
[28] A.P. Kuznetsov, S.P. Kuznetsov, E. Mosekilde, N.V. Stankevich, Generators of quasiperiodic oscillations with three-dimensional phase space, Eur. Phys. J. Spec. Top. 222 (10) (2013) 2391–2398.
[29] V. Anishchenko, S. Astakhov, T. Vadivasova, Phase dynamics of two coupled oscillators under external periodic force, Europhys. Lett. 86 (2009) 30003.
[30] V. Anishchenko, S. Nikolaev, J. Kurths, Bifurcational mechanisms of synchronization of a resonant limit cycle on a two-dimensional torus, Chaos 18 (2008) 037123.
[31] V.S. Anishchenko, S.M. Nikolaev, J. Kurths, Peculiarities of synchronization of a resonant limit cycle on a two-dimensional torus, Phys. Rev. E 76 (2007) 046216.
[32] N.V. Stankevich, J. Kurths, A.P. Kuznetsov, Forced synchronization of quasiperiodic oscillations, Commun. Nonlinear Sci. Numer. Simul. 20 (1) (2015) 316–323.
[33] H. Broer, C. Simò, R. Vitolo, Quasi-periodic bifurcations of invariant circles in low-dimensional dissipative dynamical systems, Regul. Chaotic Dyn. 16 (1–2) (2011) 154–184.
[34] M. Komuro, K. Kamiyama, T. Endo, K. Aihara, Quasi-periodic bifurcations of higher-dimensional tori, Int. J. Bifur. Chaos 26 (7) (2016) 163001.
[35] H. Broer, C. Simó, R. Vitolo, The Hopf-saddle–node bifurcation for fixed points of 3D-diffeomorphisms: the Arnol'd resonance web, Bull. Belg. Math. Soc. 15 (5) (2008) 769–787, Reprint.
[36] N.V. Stankevich, O.V. Astakhov, A.P. Kuznetsov, E.P. Seleznev, Exciting chaotic and quasi-periodic oscillations in a multicircuit oscillator with a common control scheme, Tech. Phys. Lett. 44 (5) (2018) 428–431.
[37] M. Rosenblum, A. Pikovsky, Self-organized quasiperiodicity in oscillator ensembles with global nonlinear coupling, Phys. Rev. Lett. 98 (6) (2007) 064101.
[38] A. Pikovsky, M. Rosenblum, Self-organized partially synchronous dynamics in populations of nonlinearly coupled oscillators, Physica D 238 (1) (2009) 27–37.
[39] M. Rosenblum, A. Pikovsky, Two types of quasiperiodic partial synchrony in oscillator ensembles, Phys. Rev. E 92 (1) (2015) 012919.
[40] A.P. Kuznetsov, S.P. Kuznetsov, I.R. Sataev, L.V. Turukina, About Landau–Hopf scenario in a system of coupled self-oscillators, Phys. Lett. A 377 (2013) 3291–3295.
[41] A.P. Kuznetsov, N.A. Migunova, I.R. Sataev, Sedova Yu. V., L.V. Turukina, From chaos to quasi-periodicity, Regul. Chaotic Dyn. 20 (2) (2015) 189–204.
[42] C. Baesens, J. Guckenheimer, S. Kim, R.S. MacKay, Three coupled oscillators: mode locking, global bifurcations and toroidal chaos, Physica D 49 (1991) 387–475.
[43] K. Kamiyama, N. Inaba, M. Sekikawa, T. Endo, Bifurcation boundaries of three-frequency quasi-periodic oscillations in discrete-time dynamical system, Physica D 289 (2014) 12–17.
[44] M. Sekikawa, N. Inaba, K. Kamiyama, K. Aihara, Three-dimensional tori and Arnold tongues, Chaos 24 (1) (2014) 013137.
[45] S. Hidaka, N. Inaba, M. Sekikawa, T. Endo, Bifurcation analysis of four-frequency quasi-periodic oscillations in a three-coupled delayed logistic map, Phys. Lett. A 379 (7) (2015) 664–668.
[46] V.S. Anishchenko, S.M. Nikolaev, Stability, synchronization and destruction of quasiperiodic motions, Nelineinaya Din. 2 (3) (2006) 267–278 (in Russian).
[47] V. Anishchenko, S. Nikolaev, J. Kurths, Winding number locking on a two-dimensional torus: Synchronization of quasiperiodic motions, Phys. Rev. E 73 (5) (2006) 056202.
[48] S. Wieczorek, T.B. Simpson, B. Krauskopf, D. Lenstra, Bifurcation transitions in an optically injected diode laser: theory and experiment, Opt. Commun. 215 (1–3) (2003) 125–134.
[49] D.A. Anchikov, A.P. Shakirov, A.A. Krents, N.E. Molevich, A.V. Pakhomov, Multi-frequency tori in wide-aperture lasers, Phys. Wave Phenom. 24 (2) (2016) 108–113.
[50] M. Wu, B.A. Kalinikos, L.D. Carr, C.E. Patton, Observation of spin-wave soliton fractals in magnetic film active feedback rings, Phys. Rev. Lett. 96 (18) (2006) 187202.
[51] A.B. Ustinov, V.E. Demidov, A.V. Kondrashov, B.A. Kalinikos, S.O. Demokritov, Observation of the chaotic spin-wave soliton trains in magnetic films, Phys. Rev. Lett. 106 (1) (2011) 017201.
[52] Z. Wang, A. Hagerstrom, J.Q. Anderson, W. Tong, M. Wu, L.D. Carr, B.A. Kalinikos, Chaotic spin-wave solitons in magnetic film feedback rings, Phys. Rev. Lett. 107 (11) (2011) 114102.
[53] A.V. Kondrashov, A.B. Ustinov, B.A. Kalinikos, Studying dynamic chaos in microwave ring generators based on normally magnetized ferromagnetic film, Tech. Phys. Lett. 42 (2) (2016) 208–211.
[54] Y.P. Emelianova, V.V. Emelyanov, N.M. Ryskin, Synchronization of two coupled multimode oscillators with time-delayed feedback, Commun. Nonlinear Sci. Numer. Simul. 19 (10) (2014) 3778–3791.
[55] V.V. Emelyanov, Y.P. Emelianova, N.M. Ryskin, The mutual synchronization of coupled delayed feedback klystron oscillators, Tech. Phys. 61 (8) (2016) 1256–1261.
[56] H. Ju, A.B. Neiman, A. Shilnikov, Bottom-up approach to torus bifurcation in neuron models, Chaos 28 (2018) 106317.
[57] A. Hohl, A. Gavrielides, T. Erneux, V. Kovanis, Quasiperiodic synchronization for two delay-coupled semiconductor lasers, Phys. Rev. A 59 (5) (1999) 3941–3949.
[58] S. Mondal, S.A. Pawar, R.I. Sujith, Synchronous behaviour of two interacting oscillatory systems undergoing quasiperiodic route to chaos, Chaos 27 (10) (2017) 103119.
[59] P.S. Landa, Nonlinear Oscillations and Waves in Dynamical Systems, Kluwer, Dordrecht, 1996.
[60] N.V. Stankevich, E.I. Volkov, Multistability in a three-dimensional oscillator: tori, resonant cycles and chaos, Nonlinear Dynam. 94 (4) (2018) 2455–2467.
[61] A. Pikovsky, M. Rosenblum, J. Kurths, Synchronization: A Universal Concept in Nonlinear Sciences, Cambridge University Press, Cambridge, England, 2003.
[62] V. Resmi, G. Ambika, R.E. Amritkar, General mechanism for amplitude death in coupled systems, Phys. Rev. E 84 (4) (2011) 046212.
[63] G.V. Osipov, A. Pikovsky, M. Rosenblum, J. Kurths, Phase synchronization effects in a lattice of nonidentical Rössler oscillators, Phys. Rev. E 55 (3) (1997) 2353.
[64] A.P. Kuznetsov, P. Roman Ju, Properties of synchronization in the systems of non-identical coupled van der Pol and van der Pol-Duffing oscillators. Broadband synchronization, Physica D 238 (16) (2009) 1499–1506.
[65] P. Emelianova Yu, A.P. Kuznetsov, L.V. Turukina, Quasi-periodic bifurcations and "amplitude death" in low-dimensional ensemble of van der Pol oscillators, Phys. Lett. A 378 (2014) 153–157.
[66] Z.T. Zhusubaliyev, J.L. Laugesen, E. Mosekilde, From multi-layered resonance tori to period-doubled ergodic tori, Phys. Lett. A 374 (25) (2010) 2534–2538.
[67] G.B. Ermentrout, Simulating, Analyzing, and Animating Dynamical Systems: A Guide to XPPAUT for Researchers and Students, SIAM, Philadelphia, 2002.
[68] H.W. Broer, G.B. Huitema, F. Takens, B.L.J. Braaksma, Unfoldings and Bifurcations of Quasi-Periodic Tori, No. 421, American Mathematical Soc., 1990.
[69] H.W. Broer, G.B. Huitema, M.B. Sevryuk, Quasi-Periodic Tori in Families of Dynamical Systems: Order Amidst Chaos, Springer-Verlag, Berlin, 1996.
[70] K. Kaneko, Doubling of torus, Progr. Theoret. Phys. 69 (1983) 1807–1810.
[71] K. Kaneko, Oscillation and doubling of torus, Progr. Theoret. Phys. 72 (1984) 202–215.
[72] G. Benettin, L. Galgani, A. Giorgilli, J.M. Strelcyn, Lyapunov characteristic exponents for smooth dynamical systems and for Hamiltonian systems; a method for computing all of them. Part 1: Theory, Meccanica 15 (1) (1980) 9–20.
[73] A. Pikovsky, A. Politi, Lyapunov Exponents: A Tool to Explore Complex Dynamics, Cambridge University Press, 2016.